BIOMICROFLUIDICS **10**, 011904 (2016)

Depth position detection for fast moving objects in sealed microchannel utilizing chromatic aberration

Che-Hsin Lin[a)] and Shin-Yu Su
Department of Mechanical and Electro-Mechanical Engineering, National Sun Yat-sen University, Kaohsiung 804, Taiwan

(Received 11 November 2015; accepted 15 December 2015; published online 19 January 2016)

This research reports a novel method for depth position measurement of fast moving objects inside a microfluidic channel based on the chromatic aberration effect. Two band pass filters and two avalanche photodiodes (APD) are used for rapid detecting the scattered light from the passing objected. Chromatic aberration results in the lights of different wavelengths focus at different depth positions in a microchannel. The intensity ratio of two selected bands of 430 nm–470 nm (blue band) and 630 nm–670 nm (red band) scattered from the passing object becomes a significant index for the depth information of the passing object. Results show that microspheres with the size of 20 μm and 2 μm can be resolved while using PMMA (Abbe number, $V = 52$) and BK7 ($V = 64$) as the chromatic aberration lens, respectively. The throughput of the developed system is greatly enhanced by the high sensitive APDs as the optical detectors. Human erythrocytes are also successfully detected without fluorescence labeling at a high flow velocity of 2.8 mm/s. With this approach, quantitative measurement for the depth position of rapid moving objects inside a sealed microfluidic channel can be achieved in a simple and low cost way. [http://dx.doi.org/10.1063/1.4939943]

I. INTRODUCTION

LabChip systems utilizing optical detection approaches have been widely used in clinical diagnosis like hematology,[1,2] gene analysis,[3–5] and other bio-analytical applications. However, the light intensity scattered or emitted from the target samples might vary with their depth positions in the microdevice. To prevent from the interfered signals caused by sample overlapping, it is crucial to hydro-dynamically separate the samples prior optical signal detection.[6] It is simple to focus the sample flow into a narrow stream line using a microfluidic chip yet it is still challenging to confine the sample flow in the third dimension (depth position). Therefore, there were usually intensity variations for the optical signals emitted from the samples located at the different Z-direction positions.[7] To achieve a better confinement for the sample flow in the depth position, Howell *et al.* constructed chevron structures in the micro-channel to focus the sample flow in horizontal and vertical plane.[8] There is also other micro-structures proposed to achieve the 3D focusing in cytometer like the sequential micro-weir structure[9] or positive dielectrophoresis.[10] However, these researches did not provide the quantitative inspections regarding the focusing performance in the reports.

Flow visualization is a typical solution for predicting and analyzing the flow pattern of a microfluidic channel by acquiring the tracks of the objects inside the microchannel.[11] This technique provides a rich information regarding the flow field, flow velocity, and flow stream line in the channel. Micro particle image velocimetry (micro-PIV) is a popular approach to resolve the spatial information for the flow inside a microfluidic device.[12–14] However, the particles used in

[a)]Author to whom correspondence should be addressed. Electronic mail: chehsin@mail.nsysu.edu.tw. Tel.: +886-7-5252000-4240. Fax: +886-946-526044.

PIV method should be labeled with fluorescence, and the spatial resolution for this method is limited by the image sensor and the lenses for image acquisition. Alternatively, the laser light sheet (LLS) was used as the diagnosed spot in conventional micro-PIV system to improve the spatial resolution.[15] However, the resolution in Z-direction was still confined by the depth of focus (DOF) of the LLS system such that it was challenging for analyzing defocusing samples. The defocusing digital PIV (DDPIV) was reported to improve the capability for detecting the defocusing objects.[16,17] This approach used three pre-calibrated pinholes to observe the de-focusing level of the passing particles. The real and virtual images and the various triangle side lengths formed by three pinholes were used as the indicators for the Z-direction position of the passing object.[18] Cierpka *et al*. also reported the use of the astigmatism effect to determine the position in Z-direction.[19] The phase singularities shift not only towards the z-axis but also far away from the geometrical focal plane due to the image aberration caused by astigmatism.[20] However, delicate image processing procedures were required for this approach. An even more delicate system of spinning disc confocal microscope was reported.[21] Confocal microscope was used to scan the microchannel, construct the optical section, and obtain the full image. The spinning disk with pinholes on it helped the confocal system to scan thousands of spots simultaneously without acquiring the optical signals of defocusing objects. A high spatial resolution of 1 μm with a flow speed of up to 0.52 mm/s was achieved.[22] However, these techniques relied on delicate optical design and complicated calculation; the discriminating resolution and throughput for particle positioning were also limited by the image capturing systems.

To develop an efficient method to precisely measure the position of rapid moving objects in a microfluidic device is important for future developments of LabChip or point-of-care diagnosis systems.[23] The reflection mirrors were embedded in a polydimethylsiloxane (PDMS) channel to determine the depth position of passing particle utilizing the captured top-view and side-view images by the embedded mirror.[24] This approach greatly eliminated the use of delicate optical components for depth detection. However, the fixation for the embedded mirror was time consuming and the alignment of the mirror also played an important role for the sensing performance. Recently, conventional fluorescence microscopy with reduced optical depth was reported for real-time fluorescence-based biosensing in a reaction-limited regime.[25] The sensing speed for the developed biofunctionalized slit was 10$\times$ faster than that of other state of the art designs. However, a nano-slit was required for this approach. Alternatively, chromatic aberration is an optical phenomenon that the light of different wavelengths exhibits different focal lengths in an axial direction. Chromatic aberration is generally considered as a drawback in optical imaging systems, since it reduces the image quality. However, this property makes chromatic aberration to become a powerful method for detecting the depth level of flowing objects. The scattered lights from the passing objects reflected the depth information under an axial chromatic aberration illumination.[26] The detection speed of the developed system was limited by the low optical efficiency of commercial spectrometer.

This research develops a new z-position measurement approach based on the chromatic aberration effect. This developed system is aimed to determine the depth of every passing object flowing in high speed, in place of analyzing the information by merging optical sections or deriving the images, and these measurements can be achieved by using the photodiode. With this approach, detecting the depth position of samples with high flowing speed is easy to achieve without the moveable scanning stage or high speed CCD camera. To further simplify the optical system and the mathematical analyzing processes, a beam splitter is used to separate scattered light into 2 paths and collected through a long and a short band-pass filters, respectively. Two high performance avalanche photodiodes (APDs) are adopted for high speed detection of the scattered lights, resulting in a high sample rate of 10^6 Hz. Therefore, the detection speed can be greatly increased without using the expensive spectrometer for optical detection. The intensity ratio of two selected wavelengths, 450 nm (blue band) and 670 nm (red band), from the scattered spectrum becomes a reliable index for the depth information of the detecting objects. Furthermore, this study also evaluates the sensing performance for using the insertion lens of a low Abbe number (PMMA) and a high Abbe number (BK7) for producing chromatic aberration. Micro-beads of different sizes and erythrocytes without fluorescence labeling are used for evaluating the performance of the developed system.

II. DESIGN AND FABRICATION

Figure 1 presents the working principle of the developed optical system for detecting the depth position of rapid moving objects. The chromatic aberration happens when a white light passes through a lens or prism as shown in Figure 1(a). The light components of different frequencies exhibit their corresponding refractive indices; a high frequency light (shorter wavelength) has a larger refractive index.[27] In this regard, the components of a mixed-wavelength light will disperse after passing a prism or lens then the lights of different wavelengths focus at different depth positions. It is noted that the degree of dispersion depends on an optical parameter of the prism or lens called Abbe number (V-number, V). In general, a lens with a lower Abbe number produces a greater chromatic aberration.[28] It means that the lens has higher Abbe number, which is able to decrease the dispersion of light, so lens with a high Abbe number is widely used in precise optical system such as microscope to eliminate distortion due to the optical aberration. In this developed system, chromatic aberration functions as the detecting principle by using the lens that has a relative lower Abbe number to produce the axial chromatic aberration along the optic axis. Figure 1(b) illustrates the design concept by applying the chromatic aberration character for detecting the z-position of objects. The plastic light stop inserted above the objective is aimed to block the zero-order light to create a dark-filed illumination environment. Therefore, the light scatter from the channel wall can be excluded such that the high S/N ratio signals can be obtained. The objective focus these dispersed light into a small spot; the detection objects flowing through the detection spot lead to scattering different wavelengths of light. The z-position of passing particles can be described by analyzing the scattered wavelengths of the objects. With this simple and novel configuration, detection of moving particles inside an embedded channel can be achieved without using any moving part to obtain high speed analyzing.

Figure 2 indicates the instrumental setup for the developed optical system. The system was established on a modified inverse microscope (Eclipse TE2000U, Nikon, Japan) equipped with a xenon lamp module as the light source for producing continuous spectra. A home-built plastic light stop and a high numerical aperture objective (CFI$_{60}$ 20×/0.75, Nikon, Japan) were adopted to produce a hollow-cone shape of light. Note that the design of the plastic light stop for producing the diascopic illumination was optimized to enhance the S/N ratio. Multi-spectral wavelength detection can be achieved without using the optical filter set such that the cost for the system can be greatly reduced. In order to increase the detection range in z-direction, an acrylic glass with a low Abbe number ($V = 53$) was used in lens1 while a BK7 lens ($V = 64$) was used

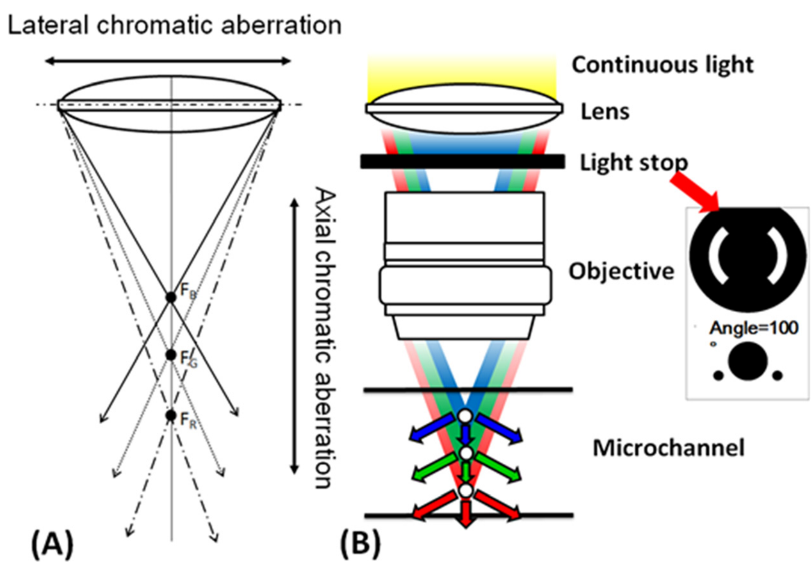

FIG. 1. (a) Schematic for the light paths of different wavelengths due to chromatic aberration. (b) Illustration of the design concept for detecting the depth position of moving particles in a microfluidic channel.

as a condenser in lens2. The scattered light from the passing samples in microchannel was collected by a low numerical aperture objective (CFI_{60} 20×/0.45, Nikon, Japan). To obtain 2 optical signals (blue and red lights), the non-polarized beam splitter cube (400 nm–700 nm, 50:50 non-beam splitter cube, ThorLabs, USA) was used, then 2 incident lights through the blue band-pass filter (SBF, CWL = 450 ± 8 nm, FWHM = 40 ± 8 nm) and red band-pass filter (SBF, LWL = 650 ± 8 nm, FWHM = 40 ± 8 nm) were used to obtain signals from blue light and red light, respectively. Two avalanche photodiodes (APD, C5460-01, Hamamatsu, Japan) were used as detectors to achieve a high flowing speed detection. The electric signals from the APDs were then captured by a DAQ card (NI USB-6259, 16 input, 16 bit, 1.25 MS/s, National Instruments, USA) via an USB interface into a personal computer. Non-fluorescence polymer beads with the size of 20 μm and diluted erythrocytes were used to demonstrate the capability of this detection technique for identifying different z-direction positions of embedded objects.

The micro-flow cytometer chip was obtained by a standard photolithography technique manufactured in the commercially available microscope glass slides and whole fabrication process as shown in Figure 3.[29] After bathing in a buffered oxide etch (BOE) etchant (6:1, J.T. Backer, USA) for 33 min, a micro-channel with the depth of 30 μm was obtained. The sample flow channel was designed with a width of 200 μm for focusing the sample stream using two symmetric sheath flows. Thus, the single inlet for the sheath flow channels with the width of 500 μm was designed for creating equal driving pressure. Note that the 150 mm cut pipette tips were utilized as reservoirs for sample and buffer solutions. Hydrodynamic pressures driven using a syringe pump were used for driving the sample and sheath flows such that the microbeads could be hydrodynamically focused at the center of the sample stream.

III. RESULTS AND DISCUSSION

Chromatic aberration is a spatial vector, and this research uses the axial chromatic aberration for detecting the depth position of the passing objects. However, the lateral chromatic aberration happens all the time such that the lateral chromatic aberration may also interfere the detection signals. To estimate the error caused by the lateral chromatic aberration, the position in Z-direction of a 10 μm bead was fixed at a reference point (the axial position is at zero-plane, $z = 0\ \mu$m), confirming that the optical signal is generated only by the axial chromatic aberration. Once the particle located at the reference point was selected, the effect caused by the lateral chromatic aberration was estimated by changing the position in X-direction and

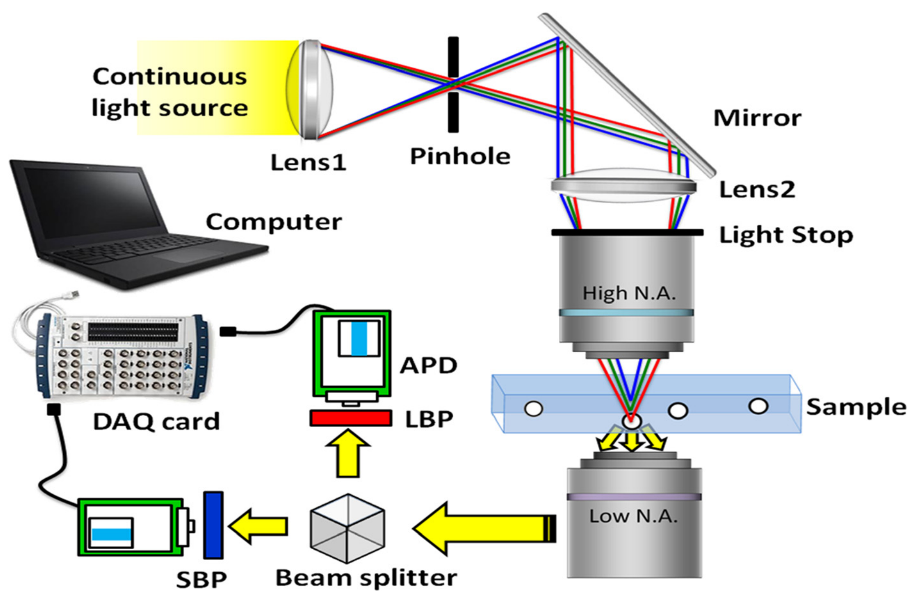

FIG. 2. A schematic showing the experimental setup for the optical system developed in this study.

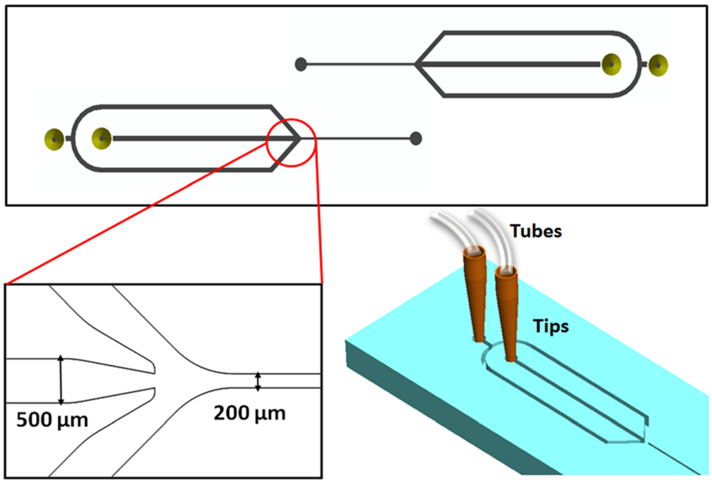

FIG. 3. The structural design for the microchip device for evaluating the sensing performance of the developed method.

recording the intensity change of short band wavelength (450 nm) and long wavelength (670 nm). In general, the lateral chromatic aberration appears in the focused spot, the size of the focused spot was about 50 μm for the developed optical system such that the maximum affected region was about $\pm$25 μm. As shown in Figure 4, the intensity of long wavelength is increasing with the off-axial distance since the long wavelength has smaller refractive index and *vice versa*. The intensity of short wavelength is gradually increasing when the X-direction position is closing to the axial one. Finally, the intensities ratio of short wavelength and long wavelength are close to 1:1 since the initial position (zero plane) was close to the region of green light. Therefore, there was only minor and insignificant enhancement in scattered blue or red ray. The variation for the measured scattered intensity (in the same axial position but different X-position, +25 μm and $-$25 μm) was only 0.136% in short wavelength and 0.434% in long wavelength, respectively. Moreover, it is easy to achieve the hydrodynamic focusing of the sample stream in the micron range for a typical micro-flow cytometer. The signal variation regarding the lateral chromatic aberration could be neglected under this scheme.

This study used the lenses of different Abbe numbers (PMMA and BK7) to create different degrees of chromatic aberration for depth detection of various particles. In general, the degree of chromatic aberration can be calculated by the following equation:

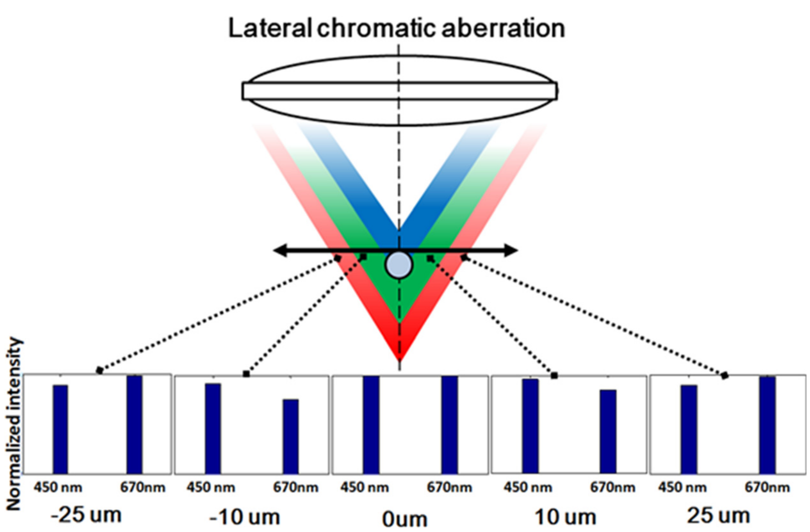

FIG. 4. Measured intensity distribution for blue band and red band signals at different X-positions.

$$\Delta f_{CF} = \sum_{i=1}^{j} \frac{Y_i{}^2}{f_i V_i}$$

where is the difference of focal length of blue light (486.1 nm) and red light (656.3 nm), y_i is the height from axial to the edge of lens for chromatic aberration (lens1 in Fig. 2), f_i is the focal length, and V_i is the Abbe number of the lens. The calculated range of chromatic aberration right after lens1 in Figure 3 for using PMMA ($V = 52$) lens was about 190.11 μm and BK7 ($V = 64$) lens was about 124.67 μm, respectively. Even if lens with a high Abbe number significantly reduced the degree of chromatic aberration, the focus of different wavelength was relatively small than lens with a low Abbe number (about 0.73 μm/nm). Results indicated that greater chromatic aberration exhibited greater depth detection range. The lens with higher Abbe number was suitable for detecting the sample of smaller size with higher spatial resolution.

Figure 5(a) illustrates the measured results for detecting particles of different sizes with PMMA lens as the aberrant component (lens1). Note that the calculated intensity ratio of 450 nm to 670 nm was used to represent the depth level. Results showed that the depth position of the particles could be resolved using the developed system. However, it is also obvious that the 2 μm particles showed only slight change on the calculated intensity ratio, resulting in a low capability for discriminating different depths (slope = 0.0003). The results confirmed that the lens with a low Abbe number showed lower capability for detecting small particles. Alternatively, the high Abbe number lens of BK7 obtained high resolving ability for detecting small particles as shown in Figure 5(b). However, the linear range for depth detection decreased to ± 10 μm due to the lower chromatic aberration level for the BK7 lens. The developed system showed its ability to discriminate the particles at different depth positions with a high spatial resolution. Note that the resolution for depth detection was also limited by the characteristic of the adopted objective lens. For a 20$\times$ objective lens used for producing the diascopic illumination, 2 μm bead is close to the resolving limit due to the low magnification. In brief, the lens with a low Abbe number could achieve higher detecting range and a high Abbe number is capable of resolving depth change of small particles.

The use of APDs as the optical detector is aimed to achieve high speed detection. However, the high optical sensitivity of APD might be interfered by scattered lights from the channel wall and cause strong background noises during detection. The scattered lights from

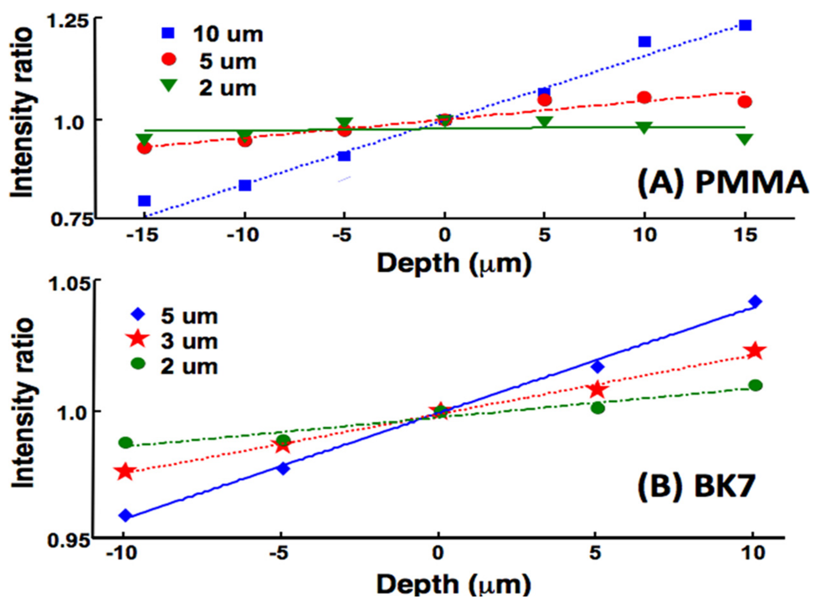

FIG. 5. (a) Depth detection of 10 μm, 5 μm, and 2 μm non-fluorescent micro-beads utilizing PMMA lens for chromatic aberration. (b) Depth detection of 5 μm, 3 μm, and 2 μm non-fluorescent micro-beads using BK7 lens for chromatic aberration.

the channel wall contained multiple wavelengths corresponding to the spectra of the tungsten-bulb light source. The scattered light from the channel wall might interfere the collected light intensities such that the calculated depth positions were also interfered. To eliminate the scattered light from the channel wall, the light stop for generating the dark-field illumination was also optimized. Two symmetrical slits were designed to prevent from the illumination of the channel wall which might cause light scattering. The sensing performance for three slit designs of 60°, 80°, and 100° were experimentally investigated. As shown in Figure 6(a), the slits with the angle of 100° caused significant illumination for the channel wall such that the scattered light reduced the linearity for the detection results. The scattered light from channel wall was obviously diminished by using the light stop with the angle of 80° and the linearity was improved (Fig. 6(b)).[30] However, there is still minor light scattering from channel wall. The slit angle of 60° provided a remarkable improvement on the detection linearity due to the eliminated light scattering from the channel wall. Moreover, the effective detecting range for the developed optical system extended to $\pm 25\,\mu$m which was 1.67-folds wider than that of $\pm 15\,\mu$m for the system using spectrometer as the optical detector.[26] This was because that the spectrometer system determined the depth level by establishing the ratio of two specific wavelengths of 450 nm and 670 nm from the captured spectra. Nevertheless, the intensity ratio was calculated the optical intensities of the blue band (430–470 nm) and red band (630–670 nm) filters, which

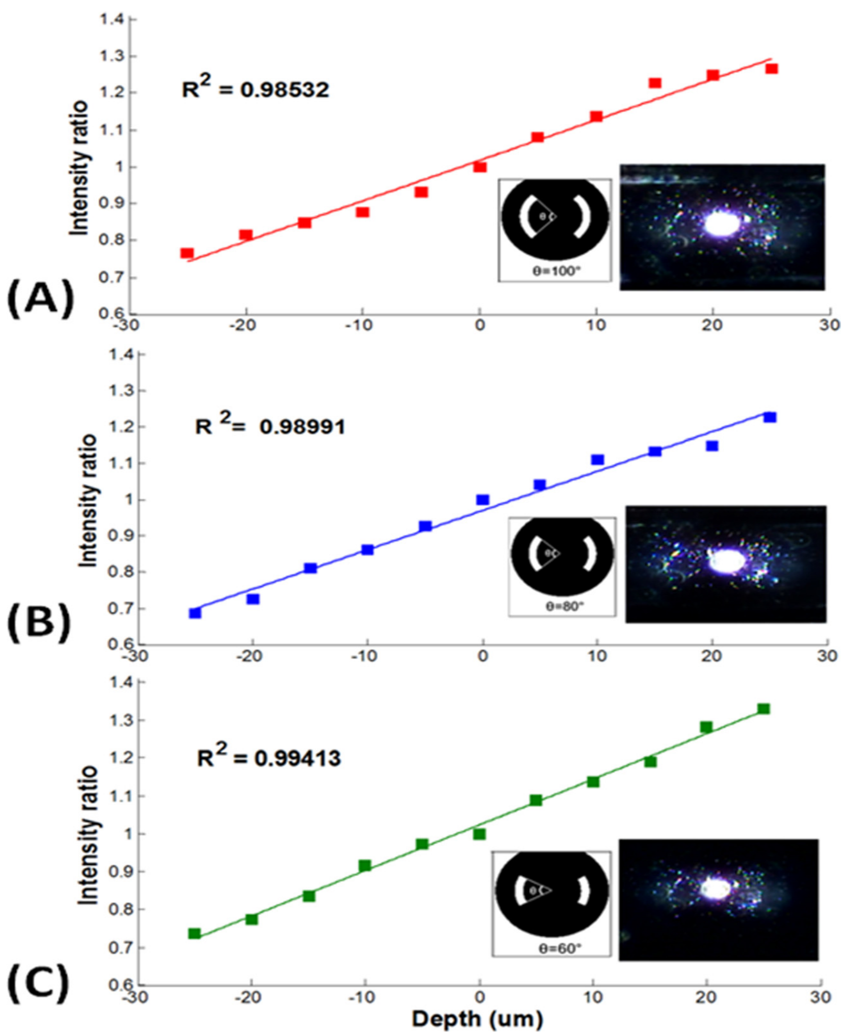

FIG. 6. Measured sensing performance for using the light-stop with (a) 100°, (b) 80°, and (c) 60° symmetrical slits.

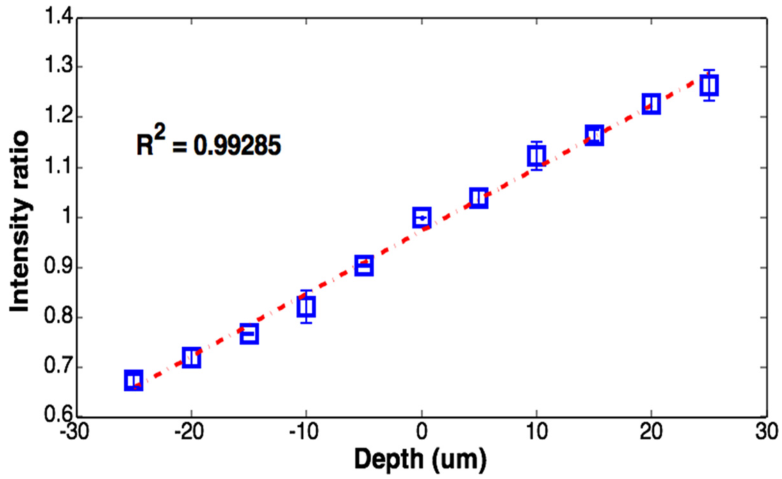

FIG. 7. Variation of intensity ratio with the particle depth given blue band and red band. Note that the error bars were calculated from the intensity ratio of 5 independent measurements.

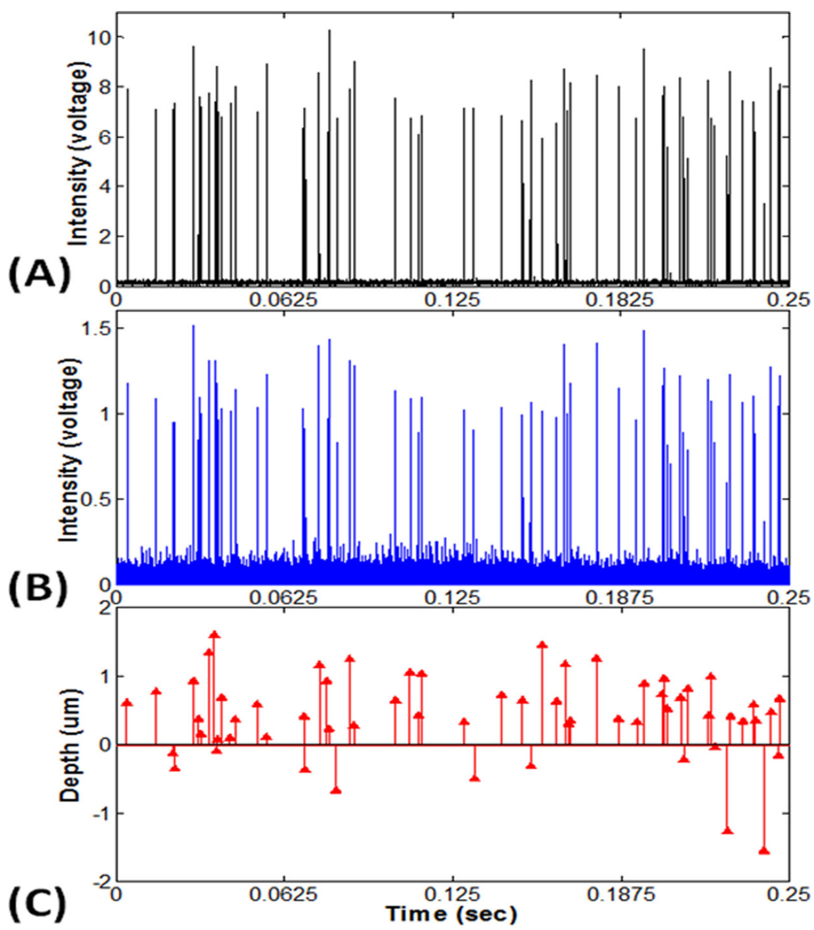

FIG. 8. Analyzing the depth levels of 20 μm microspheres under the flow velocity of 4.17 mm/s. (a) red band signals (630–670 nm), (b) blue band signals (430–470 nm), and (c) the calculated depth level for each passing microsphere.

well indicated the change of intensity in the comprehensive regions (blue and red bands). As a result, the intensity ratio was more reliable to reveal the depth level of the objects. Figure 7 shows the variation of the intensity ratio of the blue band and red band with changes in the object depth. The results confirm that a good linearity exists between the intensity ratio and the z-position of the moving objects. The results show that in a confined microchannel, the linear detection range is around $\pm 25\,\mu$m due to the lowered S/N ratio of the signal caused by scattering from the channel walls. Noted that the PMMA lens was used for this test and the standard deviations were calculated from 5 individual measurements.

A micro-flow cytometer was used to verify the capability of the developed system for dynamically depth position detection of rapid moving particles. The hydrodynamic focusing was adopted to confine the flowing stream in X-Y plane to reduce the lateral chromatic aberration. The sample solution composed of $20\,\mu$m non-labeled particles was prepared with the concentration of approximately 5×10^6 beads/ml. The flow cytometer was driven with a flow rate of $1.50\,\mu$l/min, resulting in a parabolic flow with the central velocity of 4.17 mm/s. The sampling rate for acquiring the high-band and low-band optical signals was set at 20 000 Hz. Prior to the test, the position of the objective lens was first adjusted and then fixed at the zero position. Figure 8(a) shows the captured red band signals (630–670 nm) scattered from the passing particles, and Figure 8(b) shows the captured blue band signals (430–470 nm). Each peak in these two figures represented a particle passing the detecting region which was similar to the

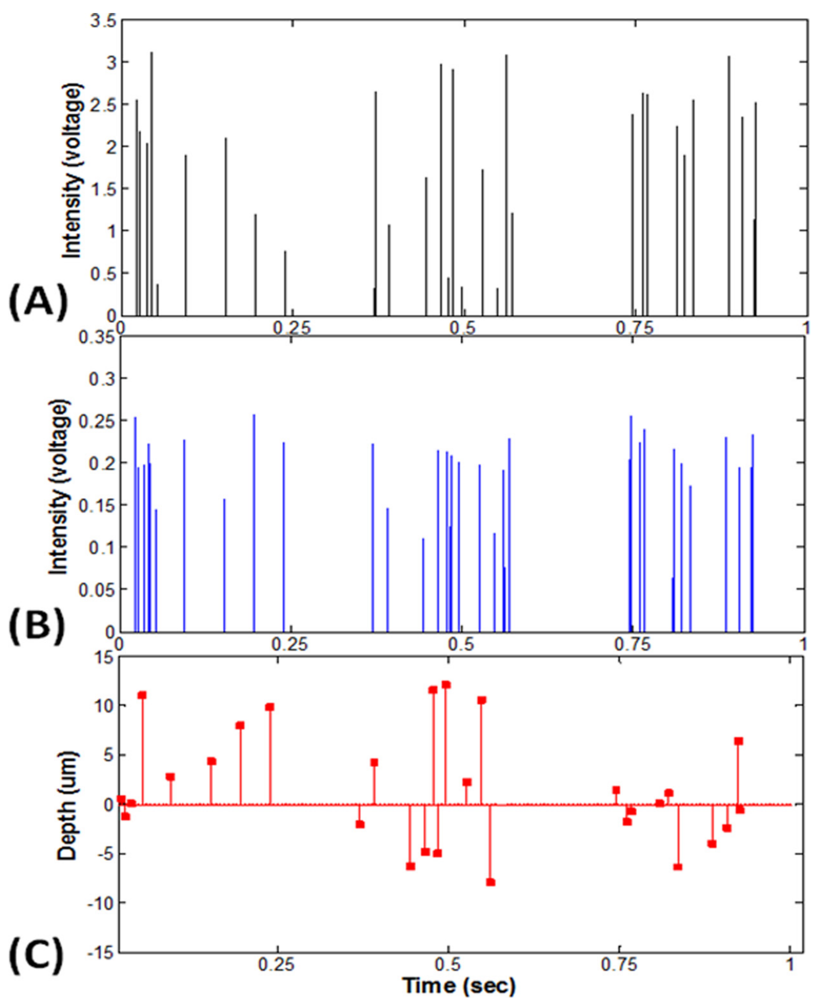

FIG. 9. Analyzing the depth levels of diluted human erythrocytes under the flow velocity of 2.78 mm/s. (a) Red band signals (630–670 nm), (b) blue band signals (430–470 nm), and (c) determined the depth positions of moving erythrocytes.

signals obtained by using a conventional flow cytometer system. Figure 8(c) shows the calculated depth levels of each corresponding signal peak presented in Figs. 8(a) and 8(b).[30] Results confirm that the developed system is capable of counting the number and detecting the depth positions of rapid moving particles simultaneously. The estimated throughput of the developed system for detecting the z-position in micro flow cytometer is 126 particle/s which was much higher than the throughput of a system using spectrometer as the optical detector (12 particles/s).[26] In addition, human erythrocyte is diluted to 2×10^3 cells/μl as normal saline was used to evaluate the developed system for detecting real cell without fluorescence labeling. The flow rate for this test was set at 1.0 μl/min, resulting in the central velocity of 2.78 mm/s. Similarly, Figures 9(a) and 9(b) illustrate the captured signals for the red and blue band scattered lights from the APDs. It is noted that the optical intensity for this test was much smaller than that of detecting the 20 μm microspheres since the size of human erythrocyte is about 6–8 μm. Figure 9(c) presents the resolved depth positions calculated with the intensity ratio of the signals from the flowing erythrocytes. It is noted that the depth of erythrocyte in micro-channel was analyzed by cross-referencing the calibration curve (7 μm). The experimental results indicated that the developed system was capable for both non-labeled microspheres and red blood cells.

IV. CONCLUSIONS

This study has successfully developed a simple yet high performance optical configuration for rapid detecting the z-direction of moving objects in an embedded channel. An objective-type dark-field illumination scheme was built to produce chromatic aberration light. The wavelengths of the scattered lights referred to the depth information of the detecting objects. Delicate moving components like electrical stage for light scanning could be excluded for depth position detection. Results indicated that the developed system exhibited an effective depth detecting range of about $\pm 25\,\mu$m, which met the most detecting range for typical microfluidic devices. With the high performance APDs as the light detectors, the depth position of rapid moving objects under the flowing velocity of 4.17 mm/s was successfully determined. This system was able to resolve 2 μm particle while using BK7 as the lens for producing chromatic aberration. The spatial resolution for the developed optical system could be further enhanced while using the objective lens with higher magnification. With this novel and simple approach, depth position determination could be achieved in a low-cost yet efficient way.

[1]S. Papakonstantinou, I. Berzina, A. Lawlor, E. J. O'neill, and P. J. O'brien, Ir. Vet. J. **66**, 6 (2013).
[2]C. H. Lin, G. L. Chang, and G. B. Lee, Int. J. Nonlinear Sci. **3**(3–4), 177–180 (2002).
[3]E. Tamiya, Bunseki Kagaku **64**(6), 397–411 (2015).
[4]E. Dekking, V. H. J. Van Der Velden, S. Bottcher, M. Bruggemann, E. Sonneveld, A. Koning-Goedheer, N. Boeckx, P. Lucio, L. Sedek, T. Szczepanski, T. Kalina, M. Kovac, P. Evans, P. G. Hoogeveen, J. Flores-Montero, A. Orfao, W. M. Comans-Bitter, F. J. T. Staal, J. J. M. Van Dongen, E. C. E. Fp6, and L. C. 018708, Best Pract. Res., Clin. Haematol. **23**(3), 333–345 (2010).
[5]M. Mirasoli, M. Guardigli, E. Michelini, and A. Roda, J. Pharm. Biomed. **87**, 36–52 (2014).
[6]A. A. Nawaz, X. J. Zhang, X. L. Mao, J. Rufo, S. C. S. Lin, F. Guo, Y. H. Zhao, M. Lapsley, P. Li, J. P. Mccoy, S. J. Levine, and T. J. Huang, Lab Chip **14**(2), 415–423 (2014).
[7]M. Nasir, D. R. Mott, M. J. Kennedy, J. P. Golden, and F. S. Ligler, Microfluid. Nanofluid. **11**(2), 119–128 (2011).
[8]P. B. Howell, J. P. Golden, L. R. Hilliard, J. S. Erickson, D. R. Mott, and F. S. Ligler, Lab Chip **8**(7), 1097–1103 (2008).
[9]H. C. Lee, H. H. Hou, R. J. Yang, C. H. Lin, and L. M. Fu, Microfluid. Nanofluid. **11**(4), 469–478 (2011).
[10]H. Chu, I. Doh, and Y. H. Cho, Lab Chip **9**(5), 686–691 (2009).
[11]M. Ichiyanagi, I. Tsutsui, Y. Kakinuma, Y. Sato, and K. Hishida, Int. J. Heat Mass Transfer **55**(11–12), 2872–2878 (2012).
[12]H. Klank, G. Goranovic, J. P. Kutter, H. Gjelstrup, J. Michelsen, and C. H. Westergaard, J. Micromech. Microeng. **12**(6), 862–869 (2002).
[13]C. Y. Chen, P. G. Menon, W. Kowalski, and K. Pekkan, Exp. Fluids **54**(1), 1426 (2013).
[14]C. Snoeyink and S. Wereley, Exp. Fluids **54**(1), 1453–1460 (2013).
[15]P. L. Knowles and K. T. Kiger, Exp. Fluids **52**(3), 697–708 (2012).
[16]S. Y. Yoon and K. C. Kim, Meas. Sci. Technol. **17**(11), 2897–2905 (2006).
[17]K. C. Kim, J. Mech. Sci. Technol. **26**(12), 3769–3784 (2012).
[18]Q. Gao, H. P. Wang, and G. X. Shen, Chin. Sci. Bull. **58**(36), 4541–4556 (2013).
[19]C. Cierpka, M. Rossi, R. Segura, and C. J. Kahler, Meas. Sci. Technol. **22**(1), 015401 (2011).
[20]Y. T. Zhang and L. Z. Pan, Opt. Laser Technol. **42**(3), 484–488 (2010).
[21]J. S. Park and K. D. Kihm, Opt. Laser Eng. **44**(3–4), 208–223 (2006).
[22]R. Lima, S. Wada, K. Tsubota, and T. Yamaguchi, Meas. Sci. Technol. **17**(4), 797–808 (2006).

[23]C. Cierpka and C. J. Kahler, J. Vis. Jpn. **15**(1), 1–31 (2012).
[24]S. Choi, S. H. Kim, and J. K. Park, Lab Chip **10**(3), 335–340 (2010).
[25]T. Leichle and C. F. Chou, Biomicrofluidics **9**(3), 034103 (2015).
[26]S. Y. Su and C. H. Lin, J. Lightwave Technol. **31**(8), 1205–1210 (2013).
[27]E. Hecht, *Optics*, 4th ed. (Addison-Wesley, Reading, Massachusetts, 2002).
[28]T. Matsuda, Y. Funae, M. Yoshida, T. Yamamoto, and T. Takaya, J. Appl. Polym. Sci. **76**(1), 50–54 (2000).
[29]C. H. Lin, G. B. Lee, Y. H. Lin, and G. L. Chang, J. Micromech. Microeng. **11**(6), 726–732 (2001).
[30]S. Y. Su, C. H. Lin, and L. M. Fu, in *Proceedings of the 19th International Conference on Miniaturized Systems for Chemistry and Life Science (MicroTAS 2015), 25–29 October 2015*.